IEEE Access
Multidisciplinary | Rapid Review | Open Access Journal

Received December 12, 2018, accepted December 24, 2018, date of publication February 1, 2019, date of current version February 12, 2019.

Digital Object Identifier 10.1109/ACCESS.2019.2892819

A Sensor Based on a Spherical Parallel Mechanism for the Measurement of Fluid Velocity: Experimental Development

GERARDO PORTILLA, ROQUE SALTARÉN, ALEJANDRO RODRÍGUEZ BARROSO, JUAN CELY, AND OZ YAKRANGI

Centro de automática y Robótica CAR UPM-CSIC, Universidad Politécnica de Madrid, 28040 Madrid, Spain

Corresponding author: Gerardo Portilla (gerardo.portilla.tuesta@alumnos.upm.es)

This work was supported in part by the Spanish Government Projects under Grant DPI2014-57220-C2-1-P, in part by the Universidad Politécnica de Madrid Project under Grant AL14-PID-15, in part by the RoboCity2030-III-CM Project (Robótica aplicada a la mejora de la calidad de vida de los ciudadanos. Fase III) under Grant S2013/MIT-2748, in part by the RoboCity2030-DIH-CM under Grant P2018/NMT-4331, in part by the Programas de Actividades I + D en la Comunidad de Madrid, and in part by the Structural Funds of the EU.

ABSTRACT In this paper, an experimental demonstration was developed, to measure the velocity of a fluid by using a sensor based on the spherical parallel mechanism with three degrees-of-freedom. This sensor transforms the kinetic energy of the fluid into potential energy by deforming the parallel mechanism. This deformation is due to the impact of the fluid on a sphere attached to the platform of the parallel mechanism. Through the acquisition of data from an inertial measurement unit in the sphere, an algorithm calculates the velocity and direction of the fluid. The mathematic model and algorithm of the velocity measurement was developed in a previous article. This paper built and tested the sensor with the objective of demonstrating the theoretical basis for the sensor. The experiment is based on the underwater movement of the sensor in a linear way along a rail. The velocity that is measured by the linear encoder is equal to the fluid's relative velocity that is measured by the sensor. The measurements taken by the encoder and the sensor were compared in three experiments. The results show that the two measurements were similar, demonstrating that the sensor can accurately measure the velocity of the fluid.

INDEX TERMS Mechanical sensor, flow sensor, parallel mechanism.

I. INTRODUCTION

In the article, "A Sensor Based on a Spherical Parallel Mechanism for the Measurement of Fluid Velocity: Physical Modeling and Computational Analysis" [1], the researchers proposed a flow sensor [1], [2] that was based on the spherical parallel mechanism with the 2 UPS + 1 RU configuration [3]. They developed a mathematic model and working algorithm for the sensor. This article develops the model into an experimental demonstration.

The sensor measures the velocity and direction of the fluid through the parallel mechanism [4]–[7], which uses passive actuators (springs). The platform of the mechanism is connected to a spherical body. Within this body, there is an inertial measurement unit (IMU). When the fluid collides with the sphere, the parallel mechanism is deformed, from which it is possible to know the angles of the platform and the acceleration of the sphere by using the IMU. These angles and accelerations are input into the algorithm that was developed previously [1]. Moreover, the velocity and direction of the fluid were calculated by using the mathematic models and the dynamics of the parallel mechanism.

The development of the proposed sensor has arisen from the need to have a real-time velocity measurement system in an underwater robot in order to control its navigation [8], [9]. Usually, the velocity of an underwater robot is measured by acoustic signals and sophisticated algorithms. Kalman filters and particle filters are used for the treatment of these signals [10], [11]. Normally, this method uses the combination of signals from an inertial navigation system (INS) and a speed log Doppler (DVL) system to provide the 3D velocity in order to control the navigation of the underwater vehicle. Theoretically, the INS/DVL signal combination requires sufficient beam measurements (at least three) to calculate

The associate editor coordinating the review of this manuscript and approving it for publication was Anuj Kumar.

the 3D velocity. However, in cases where the DVL only has limited beam measurements (less than three), the slightly coupled navigation system can no longer function, and only the INS works. Therefore, navigation error accumulates over time [12]. The proposed sensor, unlike the usual acoustic methods, works on the conversion of kinetic energy into pressure.

A. CONTRIBUTION

The development of the experiment is based on the design, construction and demonstration of the sensor. The contribution of this article validates the proposed theoretical parallel mechanism, and it is able to calculate the velocity of the fluid. Regarding the application of the sensor, it is expected that it would have a very significant impact in underwater robot use.

B. OUTLINE

The authors have divided the article into four sections. Section 2 describes the sensor, as well as the mathematic models, the algorithm of the sensor, the sensor construction, and the experimental testing. Section 3 shows the results of the experimentation, and Section 4 presents the conclusion of the obtained results.

II. MATERIALS AND METHODS

A. SENSOR DESCRIPTION

Fig. 1(a) shows the sensor and its three important parts: the sphere, neck, and the parallel mechanism. The sphere is hollow, inside of which there is an IMU. When the fluid drags the sphere, the IMU calculates the inclination angles and the acceleration of the sphere, as seen in Fig. 1(a). The inclination angles are transmitted through the neck to the parallel mechanism. It has three degrees-of-freedom (see Fig. 1(b)), with 2 UPS + 1 RU configuration. Additionally, there are three passive actuators: two prismatic (L_1 and L_2) and one rotational (A_1).

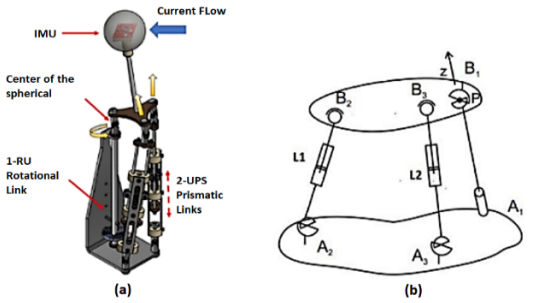

FIGURE 1. a) The sensor and its parts, the sphere, the sensor's IMU, and the parallel mechanism. (b) The parts of the parallel mechanism. L_1 and L_2 are the prismatic passive actuators, and A_1 is the rotational passive actuator. A_2, A_3, and B_1 are the universal joints, and B_2 and B_3 are the spherical joints. P is the center of the spherical motion.

These actuators are passive due to their usage of springs. The joints of the parallel mechanism include three universal joints (B_1, A_2, and A_3): one on the rotational actuator and two on the base of the prismatic actuator. Also, it has two spherical joints (B_2 and B_3) on the prismatic actuators.

The working method of this sensor is as follows. When the fluid drags the sphere, it deforms the parallel mechanism by using the IMU. In this way, it is possible to know the inclination angles of the parallel mechanism platform. By using inverse kinematics, the deformation of the springs is calculated. Knowing the deformation of the springs, the force of each actuator can be known. Then, by using dynamics, the drag force in the sphere is calculated. Finally, the velocity of the fluid is calculated by the hydrodynamic equation of the drag force.

B. MATHEMATIC MODEL

Fig. 2 shows a simplified diagram of the parallel mechanism, where the axes of the coordinates in Joint 1 can be seen. It should also be noted that the triangle of the platform is an isosceles. The line between 1 and 2 represents the rotation joint (M), and the lines between 3 and 4 (L_1) and between 5 and 6 (L_2) show the passive linear actuators.

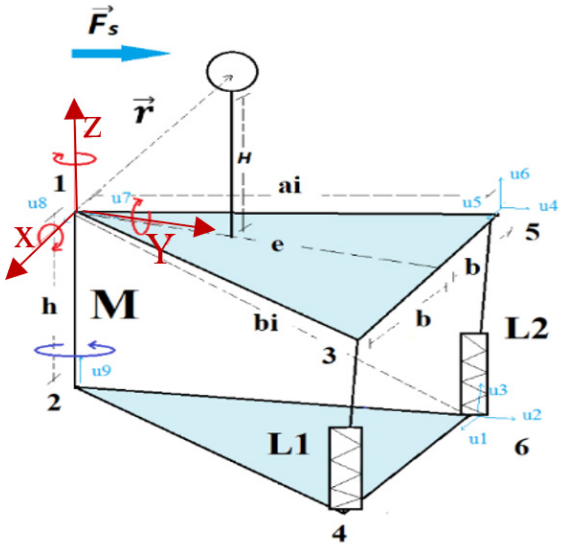

FIGURE 2. Simplified diagram of the parallel mechanism, where the plane triangles are isosceles, and the line of the length "e" is the median of the triangle. The sphere is also shown, and within it is the IMU. $\vec{F_S}$ is the force resulting from the fluid dynamic forces, and $\vec{r}$ is the center vector of the coordinates and the IMU.

1) INVERSE KINEMATIC

In order to develop the inverse kinematics, the position of each joint is calculated with a rotation matrix [13], [14], they are calculated in the frame of X, Y, and Z and are reference located in Joint 1.

After the calculation of each point, it is possible to obtain:

$$\begin{bmatrix} x_3 \\ y_3 \\ z_3 \end{bmatrix} = R\left(q_x, q_y, q_z\right) \begin{bmatrix} b \\ e \\ 0 \end{bmatrix},$$
$$\begin{bmatrix} x_5 \\ y_5 \\ z_5 \end{bmatrix} = R\left(q_x, q_y, q_z\right) \begin{bmatrix} -b \\ e \\ 0 \end{bmatrix} \quad (1)$$

where q_x, q_y, and q_z are the angles of the platform orientation in Joint 1. Therefore, the actuator would be determined by the following equations:

$$L_1 = \sqrt{(x_3 - x_4)^2 + (y_3 - y_4)^2 + (z_3 - z_4)^2} \quad (2)$$

$$L_2 = \sqrt{(x_5 - x_6)^2 + (y_5 - y_6)^2 + (z_5 - z_6)^2} \quad (3)$$

$$M = q_z \quad (4)$$

In this way, the displacements of the actuators L_1 and L_2 and the rotation of M are calculated depending on the orientation angles.

2) JACOBIAN MATRIX

The Jacobian matrix was performed by using screw theory [15]–[18], which relates the angular velocity of the spherical motion center (Joint 1) with the velocity of the passive actuators:

$$J = \begin{bmatrix} (a_1 x u_{3,1})^T \\ (a_2 x u_{3,2})^T \\ u_9^T \end{bmatrix} \quad (5)$$

where a_1,a_2 are the distances from Joint 1, to Joints 3 and 5, respectively. $u_{3,1}$, $u_{3,2}$ are the unitary vectors of actuator L_1 and L_2, respectively and u_9 is the unitary vector of Joint M.

3) DYNAMIC FORCES IN THE SPHERE AND VELOCITY

The forces applied to the sphere due to the movement of the fluid are calculated by equation (6). The calculation has previously been explained in full detail [1].

$$[r]_x^{-1}\left(J^T\tau + F_p + \sum_{i=1}^{2}\left(J_{i1}^T F_{i1} + J_{i2}^T F_{i2}\right) + J_3^T F_3\right) - m_s\vec{g}\lambda_s - \left(m_s + m_s'\right)\vec{a}_s = \vec{f}_a \quad (6)$$

where $\vec{r}$ is the vector from the frame reference center to the sensor's IMU (see Fig. 2) . The equation can be rearranged as an antisymmetric matrix, where J is the Jacobian matrix of the parallel mechanism, τ is the forces and torques vector of the actuators, F_P is the platform force, J_{i1}^T is the Jacobian matrix of the link i of Actuator 1, F_{i1} is the actuator cylinder force i, J_{i2}^T is the Jacobian matrix of the link i of Actuator 2, F_{i2} is the actuator piston force of link i, J_3^T is the Jacobian of the rotational actuator in Joint 2, and F_3 is the torque of the rotational actuator in Joint 2.

The m_s is the mass of the sphere, m_s' is the added mass by the fluid in the sphere, $\vec{a}_s$ is the acceleration vector of the sphere that is obtained by the IMU, $\vec{f}_a$, is the fluid drag force vector in the sphere, and λ_s is the density relationship between the sphere and the fluid.

Finally, the velocity is calculated by equation (7) from the fluid drag force [19]–[22]:

$$v = \sqrt{\frac{|f_a|}{C_D 0.5\rho A}} \quad (7)$$

where C_D is the drag coefficient of the sphere, ρ is the fluid density, and A is the cross-sectional area of the sphere.

As the force vector is equal to the vector of the velocity, the velocity vector is calculated by the product of the absolute velocity and the unitary vector of the force, as follows:

$$\vec{v} = v.\hat{f}_a \quad (8)$$

where $\hat{f}_a$ is the unitary vector of $\vec{f}_a$.

4) ALGORITHM FOR THE SENSOR

Fig. 3 shows the algorithm for calculating the velocity and direction of the fluid through the parallel mechanism, by using the mathematic models described in this article. The algorithm begins by entering the constants, such as inertias, masses, spring proprieties, and geometry. Next, the values of the angles and acceleration that are measured by the IMU are obtained. Then, the spring displacement of each passive actuator is calculated by using the inverse kinematic equations (see Equations (2)-(4)). The Jacobian matrix

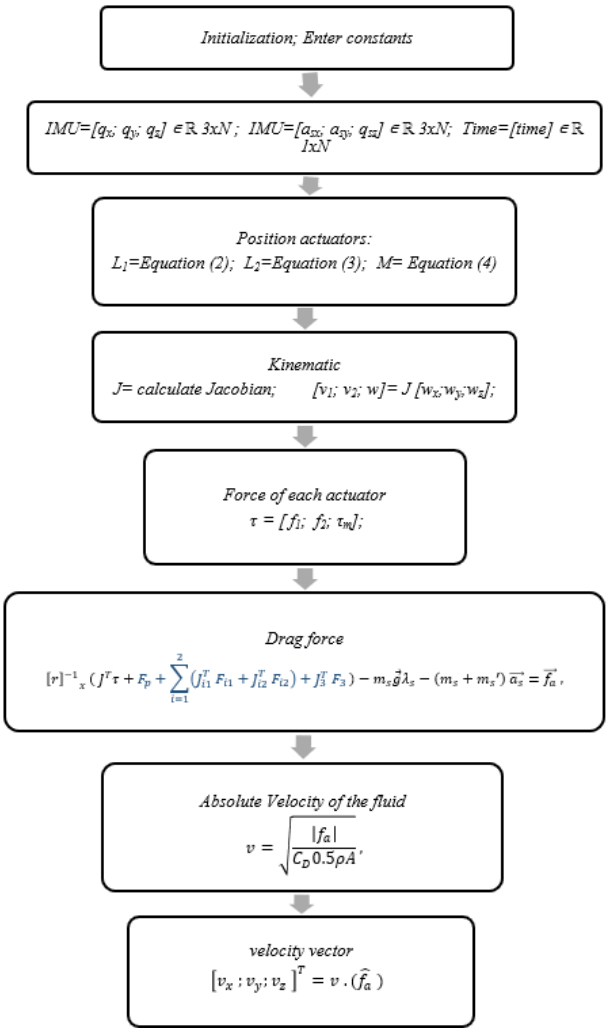

FIGURE 3. The algorithm for calculating the velocity of the fluid from the angles and acceleration that are obtained by the IMU.

(see Equation (5)) and the velocity of each actuator are also calculated. Finally, with these data, it is possible to calculate the force and torque of the actuators.

Next, the algorithm calculates the drag force from the dynamic equation (see Equation (6)). Note that the blue part of the equation represents the dynamic forces due to the inertia of the parallel mechanism. If the inertia of the mechanism is very low with respect to the drag force, it is possible not to consider this part of the equation, due to the very low forces that will generate the inertia of the mechanism. However, it should only be done if it is necessary to reduce the computational cost.

After obtaining the drag forces vector, the velocity can be calculated from the hydrodynamic equations (see Equations (7, 8)).

C. SENSOR CONSTRUCTION

Fig. 4 shows the design of the sensor in CAD. It is possible to see the 2-UPS prismatic links and the 1-RU rotational link. Also, the two IMUs are shown, IMU 1 is in the center of the sphere and IMU 2 is in the base of the sensor. The IMUs calculate the absolute angle. The sensor works by considering the relative angles in the center of the spherical motion, and so for this reason, two IMUs are necessary.

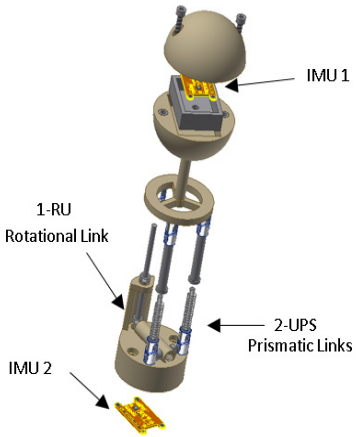

FIGURE 4. CAD design of the sensor. IMU1 is in the sphere of the sensor, and IMU2 is in the base of the sensor. Also, the 2-UPS prismatic links and 1-RU rotational link are shown.

Fig. 5 shows the real model of the sensor submerged under the water. The base and the sphere were built by ABS (Acrilonitrilo Butadieno Estireno). Fig. 5 also indicates the center of the spherical motion and the three springs. Springs 1 and 2 of the lineal joints have an elastic constant $k_L = 121\ N/m$.

Thus, the forces of the passive lineal actuator are determined by the equations below [23], [24]:

$$f_1 = -\Delta L_1 k_L \tag{9}$$

$$f_2 = -\Delta L_2 k_L \tag{10}$$

Spring three has an elastic constant $k_m = 1328\ N/m$ and is connected to the axis as shown in Fig. 6.

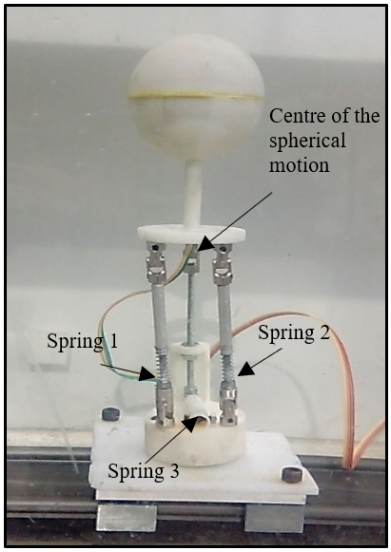

FIGURE 5. The real model of the sensor submerged in water, highlighting the three passive actuators where each spring is indicated. Also, the sphere and the base anchored to the rail are clearly visible.

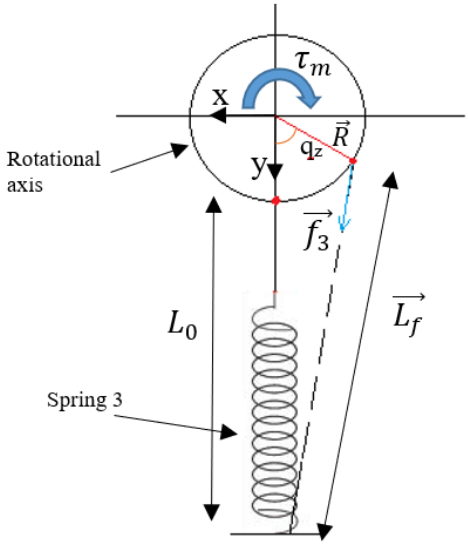

FIGURE 6. A simplified model of the connection between spring 3 and the rotational axis. This connection permits the conversion of the linear force of spring 3 to the torque in the axis.

Fig. 6 shows the simplified model of the connection between spring 3 and the rotational axis. In this way, the linear force of the spring converts into a torque. When the rotational axis rotates q_z degrees, the spring deforms up to $\vec{L_f}$ and force $\vec{f_3}$ is generated. The vector $\vec{L_f}$ is calculated by

$$\vec{L_f} = (R\,sin\,(q_z)\,,\,((R+L_0) - R\,cos\,(q_Z))\,,\,0)^T \tag{11}$$

where R is the rotational axis radius and q_z is the orientation angle in the Z-axis of the platform. The vector $\vec{R}$ is determinated by the following equation:

$$\vec{R} = (Rsin\,(q_z)\,,\,Rcos\,(qz)\,,\,0)^T \tag{12}$$

The deformation variation of the spring is determined by

$$\Delta L = \left\| \vec{L}_f \right\| - L_0 \tag{13}$$

So that the force $\vec{f}_3$ is determined by

$$\vec{f}_3 = (-\Delta L k_m) x \hat{L}_f \tag{14}$$

where $\hat{L}_f$ is the unitary vector of $\vec{L}_f$. Finally, the torque of the rotational axes is determined by [25] and [26]:

$$\tau_m = \left\| \vec{R} x \vec{f}_3 \right\| \tag{15}$$

The forces and torque vector of the actuator platform of the parallel mechanism is shown below:

$$\tau = \begin{vmatrix} f_1 \\ f_2 \\ \tau_m \end{vmatrix} \tag{16}$$

In the end, the geometric values and masses of the sensor are presented in Table 1.

TABLE 1. Geometric values and masses.

Geometry (mm)	Masses (kg)	Spring Constants (N/m)
$L_1 = 100$ $L_2 = 100$ h = 100 H = 28 b = 15 a = 41 R = 4 Diameter of the sphere = 62	$m_s = 0.18$ $m_s =$ 0.0625	$k_L = 121$ $k_m = 1328$

D. TANK CONSTRUCTION

A sensor demonstration system was built as shown in Fig. 7. The sensor is located on a rail that permits it to move horizontally through a water tank with dimensions of 800 × 800 × 300 mm. Moreover, a cord is connected to the base of the sensor, to allow the sensor to move, and is also connected to the linear encoder [27]. When the sensor moves, its displacement is equal to the displacement of the linear encoder, due to the connection by the cord. In this way, the velocity of the sensor is measured.

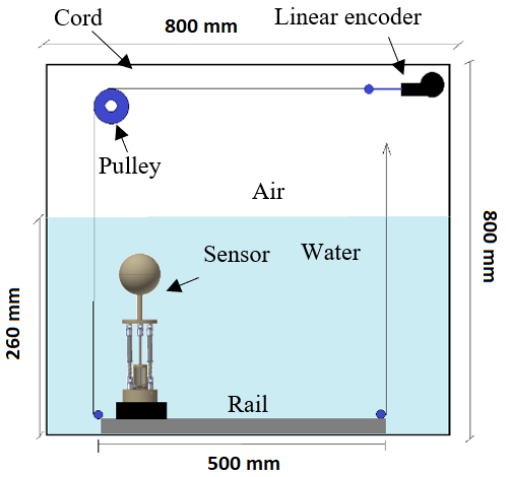

FIGURE 7. Scheme of the water tank used for the experimental demonstration. The tank is filled up to 260 mm with water. The base of the sensor is located on the rail and is permitted to move; the velocity of this movement is measured with a linear encoder and is compared with the measured velocity of the sensor, since the movement velocity of the sensor is equal to the velocity of the fluid that is measured in the opposite direction.

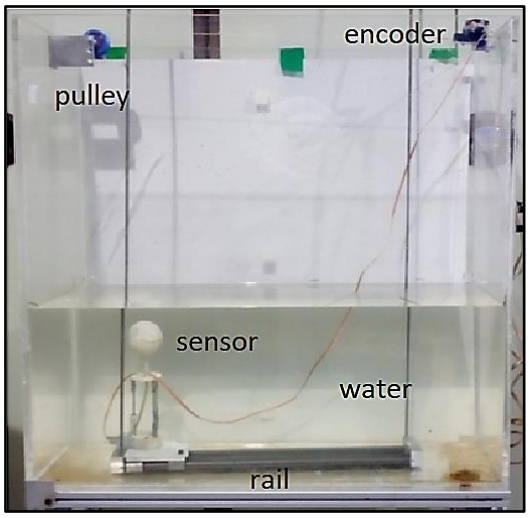

FIGURE 8. The water tank used for the experimental demonstration of the sensor. The encoder, the pulley, the sensor, the water, and the rail are shown. It is not possible to see the cord in the photo due to the low visibility of nylon in the photograph.

Fig. 8 shows the real model of the system, it is possible to see the sensor submerged in the water, the rail, the linear encoder, and the pulley. The cord is made from nylon, and for this reason, it cannot be seen. The linear encoder is an LX-EP-40 from UniMeasure. The measured resolution of the encoder was 2.4 ± 0.35% count/mm, with a precision of 0.4 mm/count. The sensing element of the encoder is an optical incremental encoder with an electrical output. It consists of two square waves, a transistor–transistor logic [28] and output channels in quadrature.

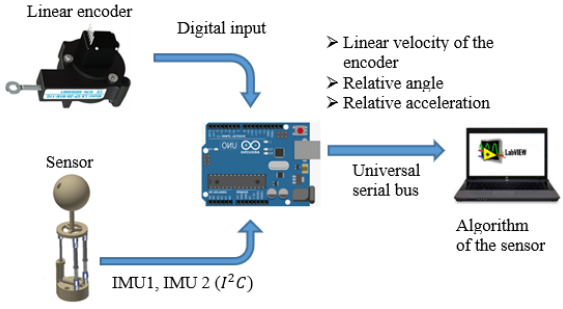

FIGURE 9. Model of the data acquisition, the linear encoder, and the sensor. Both were obtained through Arduino Uno and were sent through USB to the computer. LabView was used to calculate the velocity of the fluid using the developed algorithm. Finally, the obtained velocity is compared with that recorded the encoder.

E. DATA ACQUISITION

The data acquisition was performed as shown in Fig. 9. The measurement of the linear encoder enters to the Arduino by the digital inputs. The measurements from IMU1 and IMU2 also enter the Arduino by a serial bus Inter-Integrate Circuit ($\mathbf{I^2C}$) [29]. In addition, the Arduino calculates the linear velocity of the encoder, the relative angles between the platform and the base of the sensor in the center of the spherical motion, and also the relative acceleration between the sphere and base of the sensor. These data through the Universal Serial Bus (USB) enters into the computer, where the algorithm (Fig. 3), developed by the software LabView is applied. Then, the velocity of the fluid is calculated and is compared with the velocity obtained by the linear encoder.

F. EXPERIMENT

The principle of the experimental demonstration is based on the movement velocity of the sensor, which is equal to the velocity of the fluid in the opposite direction. The linear encoder measures the base velocity of the sensor, which is the real velocity of the fluid, and it is compared with the calculated velocity of the sensor. In this way, it is possible to determine if the sensor is able to measure the velocity of the fluid. Three experiments based on the direction of the hydrodynamic force were performed [22].

1) FIRST EXPERIMENT

The first experiment is in the direction of the hydrodynamic force along the x-axis of the parallel mechanism framework. Fig. 10 shows the sensor position in order to obtain this effect. The movement direction is matched by the x-axis of the parallel mechanism. The experiment consists of an oscillatory movement of the sensor on the rail.

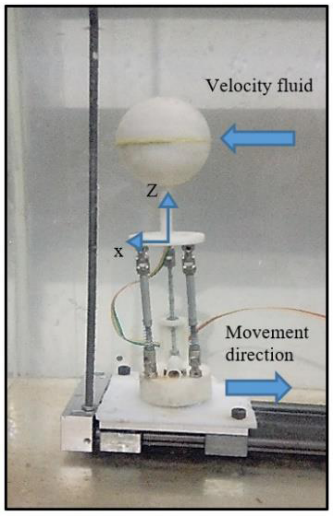

FIGURE 10. Arrangement of the sensor to show the set-up for the first experiment. The x-axis of the framework of the sensor (in the center of spherical motion) is parallel to the direction of movement of the sensor's base; in this way, the velocity of the encoder is equal to the fluid's velocity.

In this case, the velocity of the fluid in the X-axis is as shown below:

$$V_x fluid = encoder\ velocity \tag{17}$$

2) SECOND EXPERIMENT

The second experiment is the direction of the hydrodynamic force along the y-axis of the parallel mechanism framework. Fig. 11 shows the sensor position in order to obtain this effect. The movement direction is matched by the y-axis of the parallel mechanism. The experiment again consists of an oscillatory movement of the sensor along the rail.

In this case, the velocity of the fluid in the Y-axis is as shown below:

$$V_y fluid = -(encoder\ velocity) \tag{18}$$

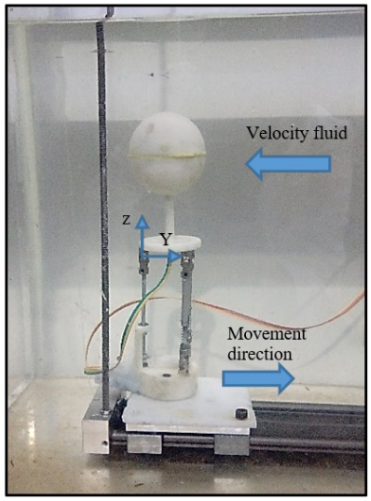

FIGURE 11. Arrangement of the sensor to show the set-up of the second experiment. The y-axis of the framework of the sensor (in the center of spherical motion) is parallel to the movement direction of the sensor's base; in this way, the velocity of the encoder is equal to the fluid's velocity.

3) THIRD EXPERIMENT

The third experiment is the direction of the hydrodynamic force between the x and z axes of the parallel mechanism framework. Fig. 12 shows the sensor position in order to obtain this effect by using a platform inclined at 30°. In the same way as the first two experiments, this experiment consists of an oscillatory movement of the sensor along the rail.

In this case, the velocities are along the X and Z axes, so that the velocity of the fluid in each axis is

$$V_x fluid = (encoder\ velocity)\ cos(30) \tag{19}$$

$$V_z fluid = -(encoder\ velocity)\ sin(30) \tag{20}$$

III. RESULTS

A. FIRST EXPERIMENT

Fig. 13 shows the oscillatory movements observed in the first experiment. Nine movements were performed over 30 s.

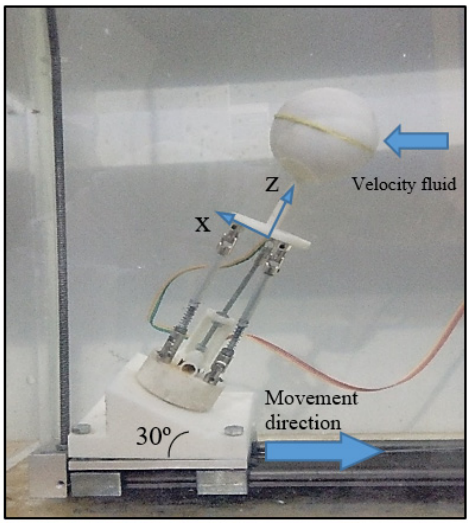

FIGURE 12. Arrangement of the sensor to show the set-up of the third experiment. The base of the sensor is inclined at 30ř , which prevents the fluid velocity to be parallel to the frame axes of the sensor reference, the velocity is calculated along the X and Z axes.

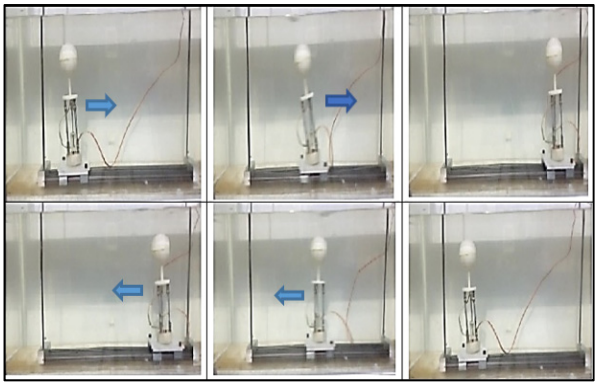

FIGURE 13. Sequence of pictures taken during the first experiment to show the sensor movement from the right to the left and vice versa for the nine movements of the experiment.

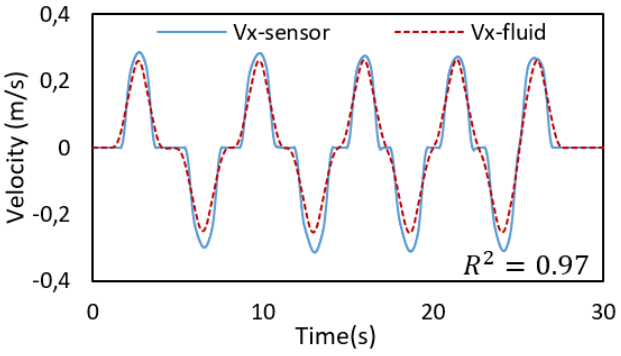

FIGURE 14. The results of the fluid's measured velocity along the x-axis by the sensor (blue line) and the encoder (red line). In this case, the real velocity of the fluid is measured by the encoder and is compared with the sensor measurement.

Fig. 14 shows the calculated velocity results of the fluid from the sensor (blue line) and the linear encoder (red line). The coefficient of determination was $R^2 = 0.97$.

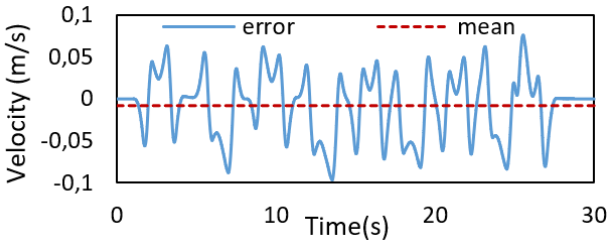

FIGURE 15. The error measurement of the sensor, with respect to the measurement of the encoder. The mean of the error is 0.008 m/s.

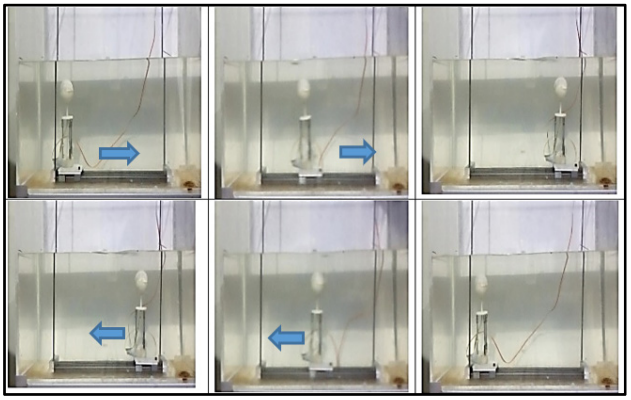

FIGURE 16. Sequence of pictures taken during the second experiment to show the sensor movement from the right to the left and vice versa, for the 10 movements of the experiment.

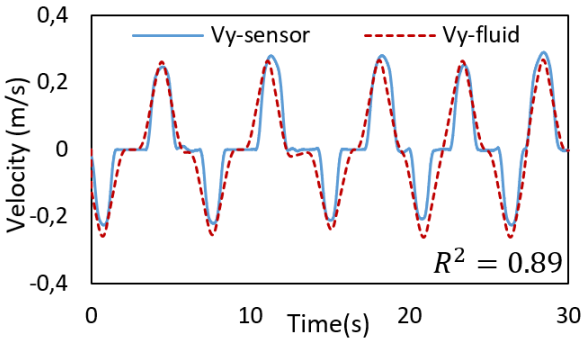

FIGURE 17. The results of the fluid's measured velocity along the y-axis from the sensor (blue line) and the encoder (red line). In this case, the real velocity of the fluid is measured by the encoder and is compared with the sensor measurement.

The absolute error of the measurement is shown in Fig. 15. The maximum error is 0.07 m/s, the minimum error is 0 m/s, and the mean is 0.008 m/s.

B. SECOND EXPERIMENT

Fig. 16 shows the oscillatory movement during the second experiment from ten movements during 30 s.

Fig. 17 shows the calculated velocity results of the fluid from the sensor (blue line) and the linear encoder (red line). The coefficient of determination is $R^2 = 0.89$.

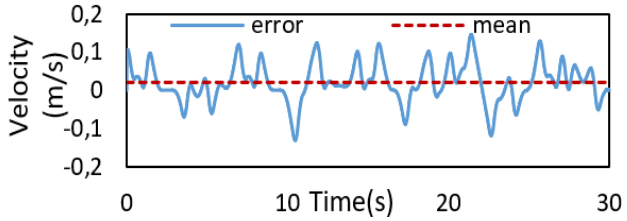

FIGURE 18. The error measurement of the sensor, with respect to the measurement of the encoder. The mean of the error is 0.02 m/s.

The absolute error of the measurement is shown in Fig. 18. The maximum error is 0.14 m/s, the minimum error is 0 m/s, and the mean is 0.02 m/s.

C. THIRD EXPERIMENT

Fig. 19 shows the oscillatory movement during the third experiment from six movements during 30 s.

Fig. 20 shows the calculated velocity results of the fluid from the sensor (blue line) and the linear encoder (red line). The coefficient of determination is $R^2 = 0.96$.

The absolute error of the measurement is shown in Fig. 21. The maximum error is 0.08 m/s, the minimum error is 0 m/s, and the mean is 0.015 m/s.

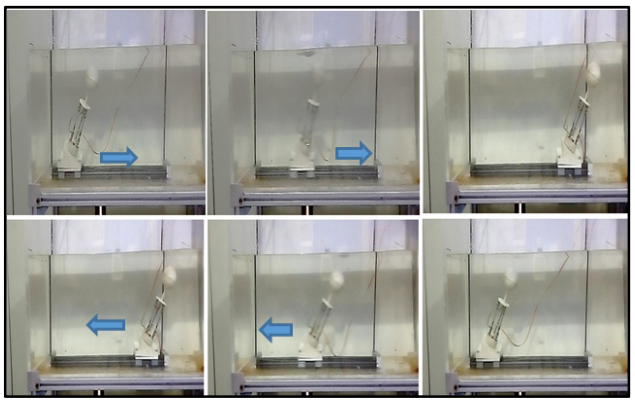

FIGURE 19. Sequence pictures taken during the third experiment to show the sensor movement from the right to the left and vice versa for the six movements of the experiment.

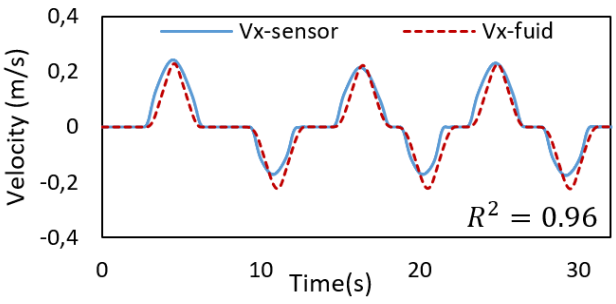

FIGURE 20. The results of the fluid's measured velocity along the x-axis from the sensor (blue line) and the encoder (red line). In this case, the real velocity of the fluid is measured by the encoder and is compared with the sensor measurement.

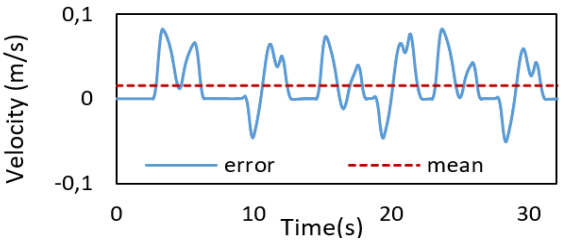

FIGURE 21. The error measurement of the sensor, with respect to the measurement of the encoder. The mean of the error is 0.015 m/s.

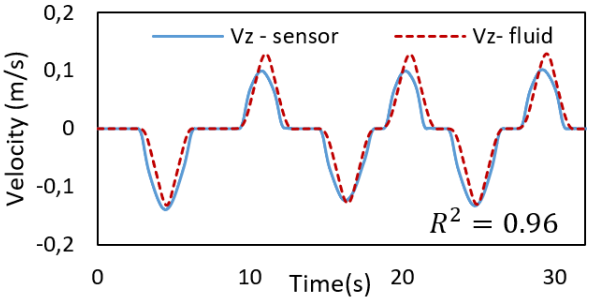

FIGURE 22. The results of the measured fluid's velocity along the Z-axis from the sensor (blue line) and the encoder (red line). In this case, the real velocity of the fluid is measured by the encoder and is compared with the sensor measurement.

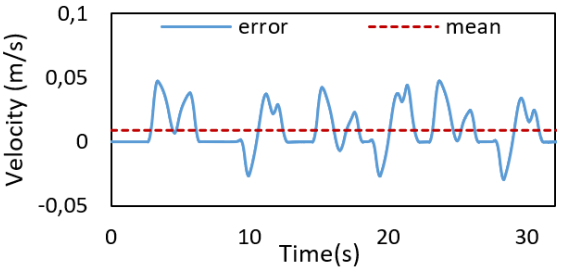

FIGURE 23. The error measurement of the sensor, with respect to the measurement of the encoder. The mean of the error is 0.009 m/s.

Fig. 22 shows the calculated velocity results of the fluid from the sensor (blue line) and the linear encoder (red line). The coefficient of determination is $R^2 = 0.96$.

The absolute error of the measurement is shown in Fig. 23. The maximum error is 0.05 m/s, the minimum error is 0 m/s, and the mean is 0.009 m/s.

IV. CONCLUSION

The results of the first experiment show that the sensor is able to measure the velocity of the fluid along the x-axis, as shown in Fig. 15. The recorded velocity values are both positive and negative, indicating the direction of the fluid flow. On one hand, the determination coefficient was $R^2 = 0.97$, which means that 97% of the fluid velocity data can be described by the data of the sensor. On other hand, the error of this measurement with respect to the fluid velocity data was obtained as an average velocity of 0.008 m/s, which represents a 9% relative error.

In the same way, the results of the second experiment (y-axis) were measured with the sensor are similar to those of the fluid velocity data. The determination coefficient in this experiment was $R^2 = 0.89$, which shows that 89% of the fluid velocity data can be described by the data of the sensor. Moreover, the error of this measurement with respect to the fluid velocity data was obtained as an average velocity of 0.02 m/s, which represents a 14% of relative error.

Finally, the measured velocities of the third experiment along the X and Z axes coincide with the measurement of the fluid velocity data. In both cases, the determination coefficient is equal and has a value of $R^2 = 0.96$, so 96% of the data of the fluid velocity data is described by the sensor. The average error on the x-axis was 0.015 m/s and on the Z-axis was 0.009 m/s; both values represent a 25% of relative error with respect to the fluid velocity data.

From the obtained results, it is possible to conclude that the sensor based on a parallel mechanism is able to measure the fluid velocity in all three spatial axes. This article presents a prototype of the sensor, and for this reason, the relative errors can be improved by further design iterations. However, from this preliminary research, the prototype is good enough to demonstrate the underlying theory.

In the future, force sensors in each actuator could be used, and in this way, the sensor would not require the IMU. Therefore, the inverse kinematics calculation would not be necessary. As a result of this change, there would be a lower computational cost.

REFERENCES

[1] R. Saltarén, G. Portilla, A. Barroso, and J. Cely, "A sensor based on a spherical parallel mechanism for the measurement of fluid velocity: Physical modelling and computational analysis," *Sensors*, vol. 18, no. 9, Aug. 2018, doi: 10.3390/s18092867.

[2] G. Neauman, *Ocean Currents*. New York, NY, USA: Elsevier, 1968.

[3] R. Saltaren *et al.*, "Performance evaluation of spherical parallel platforms for humanoid robots," *Robotica*, vol. 25, no. 3, pp. 257–267, 2006.

[4] V. Gough and S. Whitehall, "Universal tyre test machine," in *Proc. Int. Tech. Congr. FISITA*, London, U.K., 1962, pp. 117–137.

[5] D. Stewart, "A platform with six degrees of freedom," *Proc. Inst. Mech. Eng.*, vol. 180, no. 1, pp. 371–386, 1965.

[6] C. M. Gosselin and J. Angeles, "The optimum kinematic design of a spherical three-degree-of-freedom parallel manipulator," *J. Mech. Transmiss. Autom.*, vol. 111, no. 2, pp. 202–207, 1989.

[7] J. Merlet, *Parallel Robots*, 2nd ed. Dordrecht, The Netherlands: Springer, 2006.

[8] C. Álvarez, R. Saltaren, R. Aracil, and C. García, "Concepción, desarrollo y avances en el control de navegación de robots submarinos paralelos: El robot remo-I," *Revista Iberoamericana Automática Inform. Ind. RIAI*, vol. 6, no. 3, pp. 92–100, 2009.

[9] R. Rundtop and K. Frank, "Experimental evaluation of hydroacoustic instruments for ROV navigation along aquaculture net pens," *Aquacultural Eng.*, vol. 74, pp. 143–156, Sep. 2016.

[10] J. Park and J. Kim, "High-precision underwater navigation using model-referenced pose estimation with monocular vision," in *Proc. IEEE/OES*, Nov. 2016, pp. 138–143.

[11] B. Zhao, M. Blanke, and R. Skjetne, "Particle filter ROV navigation using hydroacoustic position and speed log measurements," in *Proc. ACC*, Montreal, QC, Canada, 2012, pp. 27–29.

[12] P. Liu, B. Wang, Z. Deng, and M. Fu, "INS/DVL/PS tightly coupled underwater navigation method with limited DVL measurements," *IEEE Sensors J.*, vol. 18, no. 7, pp. 2994–3002, Apr. 2018.

[13] K. Kanatani, *Understanding Geometric Algebra*. New York, NY, USA: CRC Press, 2015.

[14] K. Fu, R. Gonzalez, and C. Lee, *Robotics: Control, Sensing, Vision and Intelligence*, 1st ed. New York, NY, USA: McGraw-Hill, 1989.

[15] L. Wen, *Robot Analysis, the Mechanics of Serial and Parallel Manipulators*. New York, NY, USA: Wiley, 1999.

[16] J. Davidson and K. Hunt, *Robots and Screw Theory*. Oxford, U.K.: Oxford Univ. Press, 2002.

[17] J. Zhao, Z. Feng, and F. Chu, *Advanced Theory of Constraint and Motion Analysis for Robot Mechanisms*. Cambridge, MA, USA: Academic, 2014.

[18] R. Saltarén *et al.*, *Robótica Aplicada*. Madrid, Spain: Dextra Editorial, 2017, pp. 314–315.

[19] R. Mott, *Mecánica de Fluidos Aplicada*. Naucalpan de Juárez, México: Pearson, 1996.

[20] A. Agrawal *et al.*, "Dynamic modeling of variable ballast tank for spherical underwater robot," in *Proc. ICIT*, Cape Town, South Africa, 2013, pp. 25–28.

[21] G. Antonelli, *Underwater Robots*. Berlin, Germany: Springer, 2006.

[22] J. Fredsoe, *Hydrodynamics Around Cylindrical Structures*. Singapore: World Scientific, 1997.

[23] W. Thomson, *Theory of Vibration With Applications*. New York, NY, USA: CRC Press, 1993.

[24] K. Ogata, *Ingeniería de Control Moderna*, 5th ed. Madrid, Spain: Pearson, 2010.

[25] R. Feastherstone, *Rigid Body Dynamics Algorithms*. Sydney, NSW, Australia: Springer, 2008.

[26] H. Taghirad, *Parallel Robots: Mechanics and Control*. New York, NY, USA: CRC Press, 2013.

[27] D. Nyce, *Linear Position Sensors: Theory and Application*. Hoboken, NJ, USA: Wiley, 2004.

[28] K. Stephan, *Analog and Mixed-Signal Electronics*. Hoboken, NJ, USA: Wiley, 2015.

[29] D. Paret and C. Fenger, *The I2C Bus: From Theory to Practice*. Hoboken, NJ, USA: Wiley, 1997.

GERARDO PORTILLA received the B.Sc. degree in mechanical electrical engineering from the Universidad Católica Santo Toribio de Mogrovejo, Peru, and the M.Sc. degree in mechanical engineering from the Universidad Politécnica de Madrid, Spain, where he is currently pursuing the Ph.D. degree with the Robotic and Intelligent Machines Research Group, Centro de automática y Robótica CAR UPM-CSIC. His research interests include legged robotics, fluid power systems, and underwater robotics.

ROQUE SALTARÉN received the bachelor's degree in mechanical engineering from the Universidad del Valle, Cali, Colombia, in 1980, the M.Sc. degree in electrical engineering from the Universidad de los Andes, Bogotá, Colombia, in 1990, and the Ph.D. degree in industrial engineering from the Universidad Politécnica de Madrid, Madrid, Spain, in 1996, where he is currently an Associate Professor and a Research Scientist Coordinator with the Group of Robots and Intelligent Machines, Centro de automática y Robótica CAR UPM-CSIC.

ALEJANDRO RODRÍGUEZ BARROSO received the B.Sc. degree in industrial engineering from the Universidad Politécnica de Madrid, Spain, where he is currently pursuing the Ph.D. degree with the Robotic and Intelligent Machines Research Group, Centro de automática y Robótica CAR UPM-CSIC. His research interests include cable-driven parallel robotics, fluid power systems, and underwater robotics.

JUAN CELY received the B.Eng. degree in mechatronic engineering from Universidad Militar Nueva Granada, Bogotá, Colombia, in 2015. He is currently pursuing the Ph.D. degree in automation and robotics with the Universidad Politécnica de Madrid, where he is also working on undersea modular robots. He was graduated with Meritorious Grade Work. He have experience in robots design, control, and simulation. He taught and supervised works in math, physics, electronics, robotics, and informatics in free courses and professionals guilds.

OZ YAKRANGI received the bachelor's degree in electrical engineering from Ariel University, Israel, in 2013, and the M.Sc. degree in energy engineering from the Universitat Politécnica de Catalunya, Barcelona, Spain, in 2017. He is currently pursuing the Ph.D. degree with the Robotics and Intelligent Machines Research Group, Centro de automática y Robótica CAR UPM-CSIC, Escuela Técnica superior de Ingenieros Industriales, Universidad Politécnica de Madrid, Madrid, Spain, where he is a Researcher.